Studying the effect of tissue properties on radiofrequency ablation by visual simulation ensemble analysis

K. Heimes[1], M. Evers[1], T. Gerrits[1,2], S. Gyawali[3], D. Sinden[4], T. Preusser[3,4], and L. Linsen[1]

[1]University of Münster, Germany   [2]RWTH Aachen University, Germany
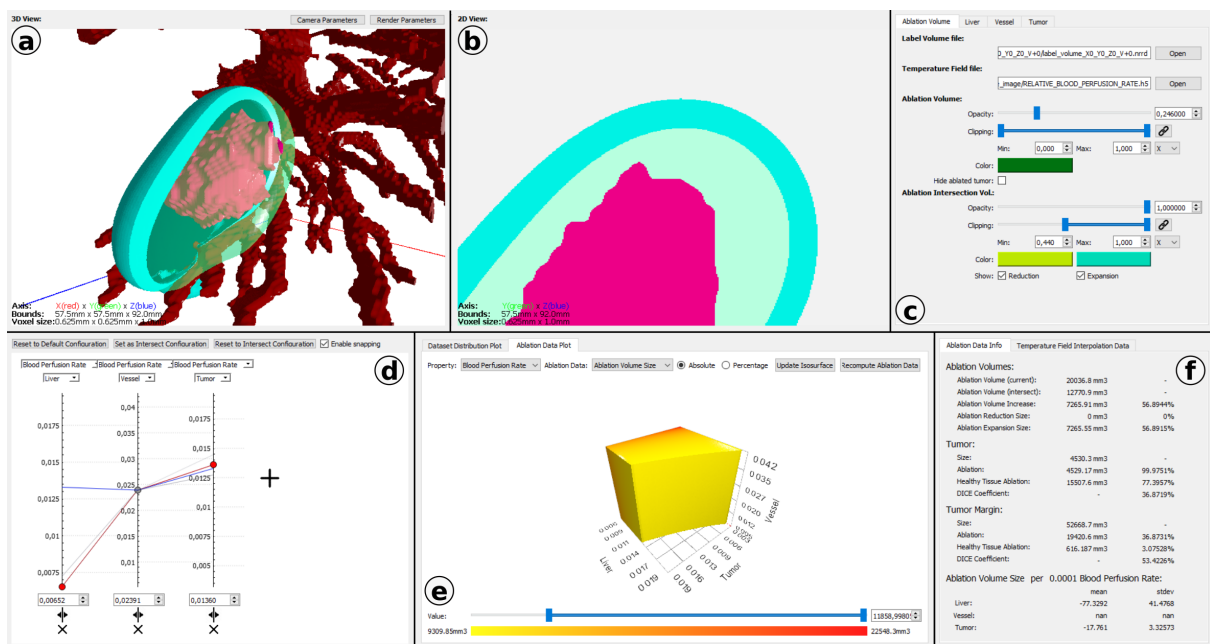[3]Jacobs University, Bremen, Germany   [4]Fraunhofer Institute for Digital Medicine MEVIS, Bremen, Germany

Figure 1: *User interface of the Tissue Property Analysis Tool (TPAT) consisting of 6 linked views. The spatial views show a 3D visualization (**a**) and a 2D visualization (**b**) of the data. Their representation can be adjusted in a separate panel (**c**). A parallel coordinates widget (**d**) allows the user to select the parameter settings of the simulation run shown in the spatial visualizations as well as for comparative visualization of two simulation runs. The ablation data plot (**e**) presents the dependencies of the outcome on the input parameters in a parameter-space visualization. Quantitative information about ablation measures is provided numerically (**f**).*

Abstract

Radiofrequency ablation is a minimally invasive, needle-based medical treatment to ablate tumors by heating due to absorption of radiofrequency electromagnetic waves. To ensure the complete target volume is destroyed, radiofrequency ablation simulations are required for treatment planning. However, the choice of tissue properties used as parameters during simulation induce a high uncertainty, as the tissue properties are strongly patient-dependent. To capture this uncertainty, a simulation ensemble can be created. Understanding the dependency of the simulation outcome on the input parameters helps to create improved simulation ensembles by focusing on the main sources of uncertainty and, thus, reducing computation costs. We present an interactive visual analysis tool for radiofrequency ablation simulation ensembles to target this objective. Spatial 2D and 3D visualizations allow for the comparison of ablation results of individual simulation runs and for the quantification of differences. Simulation runs can be interactively selected based on a parallel coordinates visualization of the parameter space. A 3D parameter space visualization allows for the analysis of the ablation outcome when altering a selected tissue property for the three tissue types involved in the ablation process. We discuss our approach with domain experts working on the development of new simulation models and demonstrate the usefulness of our approach for analyzing the influence of different tissue properties on radiofrequency ablations.

1. Introduction

With cancer being one of the leading causes of death in today's world, medical research on cancer prevention and treatment gets more and more important. Modern treatment plans have a high success rate but are not perfect yet due to the human body being a complex system and every human being different. One of these treatments is radiofrequency (RF) ablation. This minimally invasive treatment ablates a malignant or dysfunctional tissue by using an alternating current to cause coagulative necrosis of the cells. It is mostly used to treat targets in the lung, liver, kidney, or bones. While being an effective treatment to remove tumorous cells, there is a risk of leaving residues. This can lead to a recurrence and spreading of these cells.

Scientists have created theoretical models of RF ablations to gain further insights into the behavior of cells exposed to alternating current [Ber06]. They use the biological properties of the involved tissues to accurately simulate an RF ablation procedure. Properties like the blood perfusion or the thermal conductivity are known to have a high impact on the size of the ablated volume and thus strongly influence the outcome of the treatment [SCTL05, ALHG08]. Understanding how tissue properties influence the RF ablation treatment is a key factor to raise its success rate and reduce the recurrence of the tumorous tissue.

We propose the *Tissue Property Analysis Tool (TPAT)* that helps scientists and researchers to analyze simulated RF ablation data to gain more insight into how various biological tissue properties affect the treatment. Based on a task analysis of the domain (Section 3), we propose an interactive visualization tool that allows the user to explore large datasets containing hundreds of RF ablation simulation outcomes (Section 4). It allows for a quantitative analysis of the ablation outcome and lets the user inspect and compare individual ablation volumes of the simulation model to examine the effect of different tissue property settings. Interpolating the generated ensemble data in parameter space allows for a continuous exploration of the tissue property values and their influence on the ablation volume in an interactive session. The tool is designed to help researchers in the field of RF ablation modeling by supporting them in the development and evaluation of their simulation models. We present different use cases for the analysis of different aspects of the data (Section 5) and evaluate our approach with simulation domain experts (Section 6).

Our main contributions can be summarized as follows:

- The design of the interactive visual analysis tool TPAT for the analysis of radiofrequency ablation simulation ensembles.
- Comparative visualization of spatial differences in ablation volume between simulation runs.
- Parameter-space visualization of ablation outcome with regard to a tissue property for all three involved tissues.
- A use case that shows how our tool can be used to analyze the impact of different tissue properties.

2. Related Work

Different approaches in the field of medical visualization tackle the tasks of using *simulations to understand medical processes*. Raidou

et al. [RCMM*16] propose a framework for the evaluation of radiotherapy data by using Tumor Control Probability (TCP) models that quantify the probability that a tumor is effectively treated. Their tool supports the quantification and exploration of data uncertainty due to imaging modalities. It also uses a sensitivity analysis of the TCP models to draw conclusions on the parameter's effects. Another uncertainty-aware visual analysis approach was presented by Ristovski et al. [RGH*19]. They use a stochastic RF ablation simulation model to deal with uncertainty of simulation parameters. They use 2D uncertainty glyphs to provide a fast data evaluation in clinical settings, while our tool targets simulation experts with more time for detailed data analysis. The work of Rieder et al. [RWS*10] also deals with RF ablations but without considering uncertainty or ensembles. They propose a traffic light color scheme called "tumor map" to visualize the ablation state of the tumor in 3D space in the clinical context. Bricault et al. [BKM*06] propose a 3D tool to analyze post-interventional CT scans of successful RF ablations. Their tool uses a semi-automated 3D segmentation process to characterize the residual tumor tissue after an RF ablation treatment.

More general approaches for the analysis of *spatio-temporal simulation ensembles* commonly use statistical properties [PWB*09, SZD*10] or clustering [PBCR11, HHB16, FKRW17, ME19, KBL19b, KBL19a]. A recent survey presents the different aspects of ensemble visualization [WHLS19]. Phadke et al. [PPA*12] propose comparative visualizations for ensemble members, but do not analyze the parameter space of large ensembles. We propose both comparative and parameter-space visualizations.

Sedlmair et al. [SHB*14] developed a conceptional framework for *parameter-space analysis*. They identify six common analysis tasks of which we especially address the sensitivity to the input parameters which are the tissue properties in our case. This investigation also relates to the analysis of parameter-induced uncertainty, because the uncertainty in tumor ablation is a key aspect of radiofrequency ablation simulation. Techniques for parameter-space analysis include radial layouts, glyph based visualizations, projections, and dimensionality reduction [BM10, BPM*15, STDS95, OKB*19]. We follow this idea of using parallel coordinates for visualizing the parameter space [OBJ15, WLSL17], but we merely use them for navigation in parameter space to select simulation runs for further analysis. For a more in-depth analysis of the dependencies of ablation metrics on the tissue properties, we propose a 3D parameter-space visualization, where the three dimensions are formed by a selected tissue property for the three tissue types involved. Evers et al. [EL22] propose to use a hyper-slicer for a distortion-free visualization of multi-dimensional parameter spaces. However, as RF ablation simulations only involve three tissues and we want to analyze continuous changes instead of partitionings, we use a less complex visualization for the parameter space. None of the presented approaches tackles a parameter-space analysis combined with domain-specific, comparative visualizations in the medical context.

3. Task Analysis

The simulation ensemble for radiofrequency ablation simulations consists of a set of simulation runs (96 to 225 runs per ensemble) which depend on different parameter values. The simulation outcome is a 3D temperature field where voxels with a temperature of 54 °C or above are considered as ablated. The parameters describe the material properties for the different tissue types. In this work, we consider 10 different properties per tissue type. We can assume that we work with three different tissue types: healthy tissue (in our case the liver), malignant or dysfunctional tissue (in our case a tumor), and blood vessels, which significantly impact the ablation process due to the cooling factor of the blood flow. To identify the positions for the different tissues, a segmented image of the regions of interest is given, which assigns different labels to the different tissue types. This segmentation is used in the simulation to assign different tissue properties to the differently labeled regions. Due to the strong spatial dependence, we do not only want to analyze the dependence on the numerical tissue property values but also on the spatial distribution of the tissue. Further, the simulation requires the position and orientation of the needle, that is used to ablate the tissue.

For the development of our analysis tool, we worked closely together with domain experts who developed the simulation tool. In regular meetings, we developed the presented tool and iteratively refined it based on the experts' feedback. At the beginning of the process, we identified a set of tasks that we aim to address with our visual analysis tool, which we list in the following:

T1: *Investigate the simulation outcome for different tissue properties*. RF ablation simulations are computed to investigate which area gets ablated. In particular, one would like to observe if the tumor gets fully ablated (typically including a safety margin) and how much the healthy tissue is affected. The user should be able to observe the simulation outcome to get familiar with the output. The different tissues like the blood vessels should be included in the visualization to provide spatial context.

T2: *Compare the shape and size of ablation volumes for different tissue properties*. To understand the influence of the tissue property on the shape and size of the ablated volume, it should be possible to explicitly compare the ablation volume for different tissue properties. This allows the user to investigate changes in the spatial distribution and influences of surrounding tissue types.

T3: *Detect the most important tissue properties*. The wide range of possible tissue properties combined with the variety of different tissues, leads to a high number of input parameters for the numerical simulations. To reduce the dimensionality of the parameter space and, thus, computational costs for creating the simulation ensemble, it is important to identify the tissue properties that have the highest influence on the outcome.

T4: *Explore how different ablation measures change with varying tissue properties.* Derived measures like the volume of the ablated tissue, the percentage of ablated tumor tissue, or the DICE coefficient are of high interest to the domain experts and are commonly used in their analyses of simulation data. They would like to investigate how these characteristic values change with varying input parameters.

4. Visual Design

To address the identified tasks, we propose the *Tissue Property Analysis Tool (TPAT)* using multiple coordinates views, see Figure 1. *Spatial visualizations* show the ablation volume for selected parameter settings in relation to the different tissues like the tumor or the vessels (Task T1), see Section 4.1. This provides the user with an overview about the spatial extent of the ablated and tissue regions. These views also allow the user to compare ablation volumes for different tissue properties (Task T2). The simulation runs shown in the spatial visualizations can be selected by the user by selecting tissue property values in *parallel coordinates*, see Section 4.2. Here, we also support a parameter-space interpolation of existing simulation runs. To quantify the influence of the properties on the ablated tissue, we include different *quantitative metrics*, see Section 4.3. To investigate the influence of the tissue properties, we propose what we call the *ablation data plot* that provides a parameter-space overview visualization of the whole ensemble for a selected tissue property and the three different tissue types blood vessel, tumor, and liver, see Section 4.4. The parameter-space volume can be explored by rendering isosurfaces that visualize the data for a selected range of values of a derived metric. This allows the user to estimate the influence of the parameters (Task T1). By using interaction, the user can also identify how the derived measure changes with varying tissue properties (Task T2). We refer to the accompanying video for a demonstration of the tool and the respective interactions with the coordinated views.

4.1. Spatial Visualizations

The *3D volume visualization* (Figure 1a) uses the data of the labeled tissue image to display tumor, liver, and blood vessel tissues. In addition, the output temperature field of the simulation is used to visualize the ablated volume by creating an isosurface for temperature value 54 °C. The user can change the viewing parameters by rotation, translation, and zooming. This view is the main tool to observe volumetric changes of the ablation area due to different tissue property values (Task T1).

The *2D volume visualization* (Figure 1b) shows the same data as the 3D view but only displays a 2D slice of the volume. The clipping dimensions and the position of the clipping plane can be set and changed interactively by the user. The 2D slice view addresses the same tasks as the 3D volume visualization, where the view is more restricted but does not suffer from occlusion. Moreover, it supports measuring distances to quantify volumetric changes on the ablation volume. Measuring distances in the slices is facilitated by right-clicking and dragging, see Figure 2, which is a common interaction in medical visualization tools and, thus, intuitively to use for domain scientists.

The user can interactively adjust the appearance of the different volumes in the rendered 2D and 3D scenes (Figure 1c). The user-defined adjustments include visual properties like color, opacity, and the position of the clipping plane for the slice viewer. Note that we visualize the tissue segmentation, i.e., the voxels belonging to the different tissues. Even though this leads to staircase patterns, a smooth isosurface might be misleading here. It is also possible to show a so-called *safety margin* around the tumor. For treatment
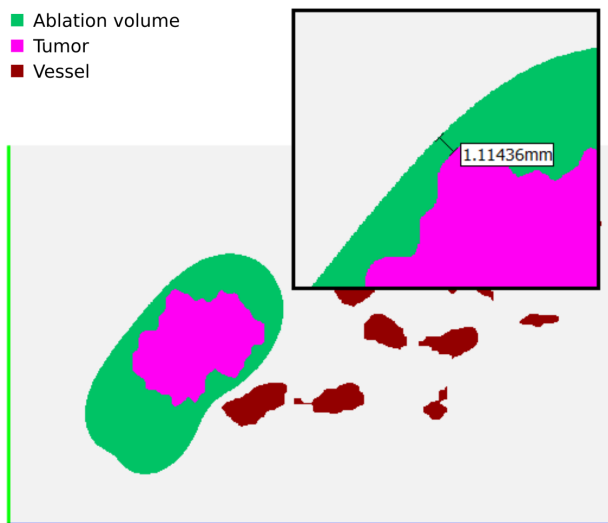
Figure 2: *Slice viewer displaying blood vessels (red), tumor (pink), and ablation area (green). The inset (black box) shows an minimum value of the margin of the treatment, i.e. the minimum distance between the tumor and the ablated volume.*

Figure 3: *Comparative visualization: Two ablation volumes for different tissue properties can be compared by calculating the expansion (blue) and reduction (red) volumes, illustrated schematically in 2D.*

duction volume by different color encodings allows us to clearly differentiate between those two changes. Thus, it can be easily observed where the ablation area increased and where it decreased, even when the differences are small. Including these volumes in the 2D and 3D volume visualizations does not only allow the user to investigate their extent in the spatial context, but also to measure their size using the slice viewer for a quantification of the expansion/reduction of the ablation volume.

4.2. Selection and Interpolation of Simulation Results

We use a *parallel coordinates widget* to select the tissue property values for their investigations in the spatial visualizations, see Figure 1d. The axes work as sliders for the corresponding parameter. Besides the selected data point, we show its k neighbors as semi-transparent grey lines. The number of neighbors k can be adjusted by the user. We choose parallel coordinates for the parameter space visualization, because they are well-suited to visualize multidimensional data, scale well with the dimensionality, and allow for an intuitive selection of values on individual axes. Selected values on the parallel coordinates' axes are then used for the spatial visualizations of the simulation outcome (Task T1) as well as for the comparative visualizations (Task T2). As the dimensionality of the parameter space is pretty high, we further improve the scalability by allowing the user to interactively select the axes that are included in the plot. For all hidden axes, a default value for the respective tissue property is chosen. The default value for the tissue properties is the average for the corresponding property, see supplementary material for the list of default values. The blue polyline displays the property values of the reference volume used for comparison, while the red polyline displays the property values of the currently selected volume.

planning, it is common practice to add a margin around the tumor tissue to account for the uncertainty in the tumor segmentation. The ablated volume should then include the tumor and the safety margin. In our tool, the user can define the size of the margin which is then shown in the spatial visualizations.

To enable a *comparative visualization* of two volumes, we compute the ablation intersection volumes (Task T2). The *ablation intersection volumes* are two volumes created by comparing the ablation volume of the current tissue property values with the volume to a reference configuration of property values. The respective values can be chosen using parallel coordinates, see Section 4.2. By this selection, we obtain two parameter value settings, for which we compare the simulation output. We refer to the calculated volumes as *expansion* and *reduction* volume. The expansion volume is the spatial region of the current ablation area subtracted by the ablation area of the reference property value configuration, where we use the set difference. This results in a new volume (possibly consisting of disconnected parts) that indicate, in which spatial regions the current volume exceeds the ablation volume of the reference configuration. The reduction volume displays the ablation area of the reference property value configuration subtracted by the current ablation area (see Figure 3) and, thus, indicates regions where the current volume is smaller than the reference volume.

Visualizing these volumes in the 2D and 3D spatial visualizations is the main tool to explore the volumetric changes on the ablation volume due to varying tissue property values. This comparative visualization is especially helpful to consider variations in the spatial domain (Task T2). Providing the spatial context by also showing the different tissues, the volume rendering shows how the distance and position of different tissues (especially vessels) influence the ablation volume's shape and sensitivity to tissue properties. The comparative visualization showing the expansion and re-
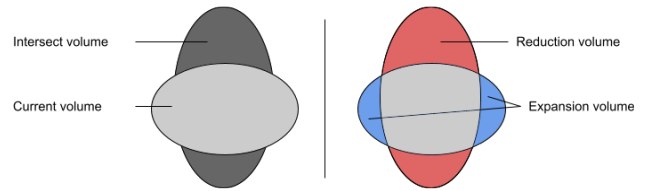
For a smooth analysis of the simulation data, a high sampling of the parameter space is needed. Since we can only compute a finite number of simulation runs, we propose to use interpolations of the temperature fields based on the parameter-value settings. Given a selected parameter setting, we use scattered data interpolation of the k nearest neighbors, where the k nearest neighbors are computed in the multi-dimensional parameter space. The k nearest neighbors are also shown in the parallel coordinates widget. For scattered data interpolation, the user may select among Shepard's method for inverse-distance-based interpolation [She68] and interpolation with radial basis functions [Buh00] using polynomials, Gaussian, or multiquadric functions. For all the results presented

in this work, we use inverse-distance-based interpolation. For the computation of the scattered data interpolation weights, the tissue properties are normalized using their possible value ranges. Then, the temperature field is interpolated using these weights and rendered in the 2D and 3D spatial visualizations.

4.3. Quantitative Information

There are a number of ablation measures that quantify various aspects of the ablation result and are commonly used by domain experts. When loading a new dataset to TPAT, the program starts to compute those metrics for each temperature field in the ensemble. These metrics include:

- *Ablation volume size*: The size of the ablation volume in mm^3.
- *Tumor volume size*: The size of the tumor in mm^3.
- *Tumor ablation volume*: The size of the tumor's volume that gets ablated in mm^3 and %.
- *Healthy tissue ablation volume*: The amount of healthy tissue that gets ablated in mm^3 and %.
- *DICE coefficient* [Dic45]: A metric to measure the similarity of two sets of data X and Y:

$$DSC = \frac{2|X \cap Y|}{|X| + |Y|} \qquad (1)$$

Here, the similarity of the ablated tumor volume X and the entire ablated volume Y gets measured, such that $|X|$ and $|Y|$ describe the number of voxels in the respective volume. Higher values for the DICE coefficient, in general, mean lower amounts of ablated healthy tissue.

- *Tumor margin volume size*: The size of the tumor plus a margin of 1 cm around it.
- *Tumor margin ablation volume*: The size of the tumor margins volume that gets ablated in mm^3 and %.
- *Healthy tissue ablation volume (margin)*: The amount of healthy tissue in mm^3 and % that gets ablated considering the tumor margin.
- *DICE coefficient (margin)*: The similarity of the tumor plus its margin and the entire ablation volume. The DICE coefficient is calculated as described in Equation 1.
- *Mean increase per tissue property unit*: The mean increase of a specific ablation measure per tissue property unit $\Phi_{abl\_data}^{tp}$ reveals what impact a certain property has on the ablation data. We also calculate the standard deviation such that the mean values with a high standard deviation can be further investigated in the visualizations to understand the parameter dependency. This metric is used within the datasets to compare the influence of the three tissue types to one another and between the datasets of the ensembles to examine changes in these values due to different segmentations or secondary property changes. The lower index *abl_data* indicates whether the ablation volume size (*abl_vol*) or the tumor ablation amount (*t_abl*) is used as ablation measure. The upper index *tp* denotes the tissue property for which this value is calculated.
- *Change of ablation volume*: The change of ablation volume Δ_{abl_data} is calculated by subtracting the minimum ablation data value of the ensemble from the maximum value and dividing the result by the average. This metric intends to describe how much the inspected tissue property in an ensemble affects the chosen ablation measure *abl_data*. It gives a quick indication whether the tissue property values have an effect at all and can be used to compare the influence of the tissue properties between different datasets.

This computed values of all measures are shown numerically in a separate panel of our tool, see Figure 1f. We also considered different design alternatives for a visual representation of the numbers. However, as the main goal is the extraction of the exact numerical values, we decided on a numerical representation. Showing the different metrics together in a visualization might also be misleading as they are rather different in their characteristics and have rather different value ranges. Thus, common visualization methods like bar charts do not add further insights but make reading off explicit values more difficult.

4.4. Parameter-space Visualizations

To find the most important tissue property (Task T3) and investigate how the ablation measure changes with changing tissue properties (Task T4), we propose to include respective parameter-space visualizations in the form of what we call the *dataset distribution plot* (Figure 4) and the *ablation data plot* (Figure 1e). This visualizations provide an overview of the whole ensemble dataset instead of single temperature fields of individual simulation runs. We visualize a 3D subspace of the parameter space by choosing one tissue property that we want to investigate further. We then show the 3D subspace spanned by the selected tissue property for the three tissue types liver, tumor, and vessel in 3D Cartesian coordinates. We can generally assume this set-up to be valid, as one generally models healthy tissue, malignant tissue, and blood vessels in RF ablation simulations.

In the *dataset distribution plot* shown in Figure 4, the parameter values for simulation runs are shown by assigning each simulation run to a point in a 3D scatterplot. The distribution of the points in the scatterplot reveals how the parameter space was sampled to generate the simulation ensemble. Each run is shown as a grey dot, but the currently selected parameter settings of the simulation run shown in the spatial visualizations is shown as a green dot. Additionally, the *k* nearest neighbors that are used for interpolation are shown as blue dots. As the visualization only shows a subspace of the parameter space, the user can interactively change the tissue property. To reduce occlusion in larger, not uniformly sampled datasets, the user can define a distance to the selected simulation run, up to which the samples should be shown. To reduce spatial orientation problems occurring in 3D scatter plots, we show a grid structure in the background. For a fast selection of a simulation run with specific parameter values, the user can select a point in the scatterplot by clicking on it. This selection is then used to update all other linked views, including the parallel coordinates and the spatial visualizations.

The *ablation data plot* shown in Figure 1e is a novel visualization method to investigate the influence of tissue properties on the ablation outcome. Its set-up is similar to the dataset distribution plot, i.e., it uses a 3D Cartesian coordinate system spanned by a selected tissue property parameter for the three tissue types. To analyze the impact of tissue properties on the ablation outcome, the
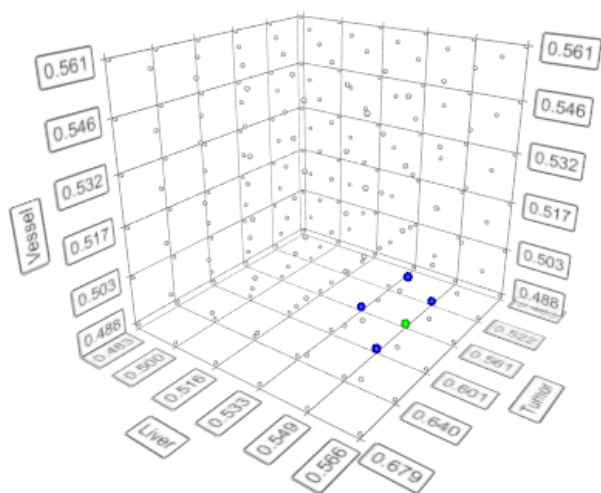
Figure 4: *Dataset distribution plot of 3D parameter subspace formed by a selected tissue property for the three tissues liver, tumor, and vessel. It shows the distribution of parameter settings of the simulation ensemble (grey), the currently selected parameter setting (green), and its k nearest neighbors (blue).*

user first selects an ablation measure (cf. Section 4.3) he/she wants to investigate. Showing the ablation measure in a 3D Cartesian coordinate system allows the user to directly visualize the domain-specific information by adapting a well-known visualization for analyzing the dependencies on the tissue properties (Task T4).

After having selected a metric, the user can interactively define an interval of the selected metric's range with a slider that is located below the plot (see Figure 1e). The plot then shows a surface in the 3D parameter subspace which surrounds all parameter settings, where the ablation measure's values lie in the chosen value range. The surface is given in the form of two isosurfaces, one for the lower and one for the upper limit of the selected interval, which then get connected along the boundary of the 3D parameter subspace to enclose all points, where the ablation measure's values are between that lower and upper limit. This surface allows the user to easily inspect where the ablation measure values are particularly high or low for the specific tissue property. Moreover, it can be used to investigate certain points of interest in the parameter space where the ablation measure suddenly responses differently to property value changes.

In addition, the surface is color-coded with respect to the ablation measure, where a color map from yellow (minimum value for the chosen metric in the whole dataset) to red (maximum value for the chosen metric in the whole dataset) is used (cf. Figure 1e). Obviously, the two isosurfaces for the lower and upper limit of the selected interval are single-colored, but along the boundary of the 3D parameter subspace one can observe a color gradient, which already provides a hint about the influence of the selected tissue property (Task T3). The change in the volume surrounded by the surface when interactively changing the selected range of the chosen metric, further supports the identification of the most important

properties. Moreover, it provides the user a fast means to observe if and how the different tissue properties of the dataset affect the ablation data metric (Task T4). The three-dimensional visualization also supports a direct comparison of the different tissues as one can see how the isosurface varies if the selected range is changed. The interactive exploration also exhibits the presence of nonlinearities by variations in the speed of change of the isosurface.

5. Usage Scenario

We applied our visual analysis tool TPAT to radiofrequency ablation data created using the thermal ablation simulation library *TAS* [KAP*06]. We systematically investigated the influence of different tissue properties as well as the variations in the spatial positions. In the following, we will first provide a detailed explanation of the datasets we created (Section 5.1), which we then used for a detailed systematic analysis. Then, we will highlight parts of our analysis results (Section 5.2) and provide some feedback from the domain experts (Section 5.3). All results of our systematic analysis can be found in the supplementary material.

5.1. Ensemble Generation and Analytical Workflow

For the analysis with our tool, we used in total four different ensembles where each focuses on one aspect. In the following, we provide the details on the different ensembles, describe the goals for their analysis, and give an overview of the analytical workflow. The exact ranges of all parameters that we used as inputs are provided in the supplementary material.

Ensemble A: The first ensemble dataset aims at investigating single tissue properties in different kinds of tissues. To keep the data size reasonable, each tissue property is varied for the three different tissue types (liver, vessel and tumor), while the other tissue properties are kept constant. After familiarizing ourselves with the volume data, we start the analysis by checking the data ranges in the ablation data plot to investigate whether the different tissue properties affect the ablation area at all. In the following, we refer to the ones who affect the ablated area as *primary tissue properties*. In our simulations, we identified that the optical and acoustic properties as well as the electric properties and the water ratio do not influence the output at all. Therefore, we neglected these tissue properties in the subsequent analysis steps. Using the surface of the ablation data plot and the precalculated ablation metrics, the datasets of the primary tissue properties were investigated in more detail. Using the spatial visualizations, the volumetric changes in the ablation volume due to different tissue property values were inspected.

Ensemble B: We use the previously gained knowledge about the primary tissue properties to examine their influence on the temperature field when a second property is changed simultaneously. Therefore, the second ensemble dataset can be used to investigate the interaction between different tissue properties. For the analysis, we follow a similar approach as above. An important statistical property for these ensembles is the difference between the maximum and minimum value of the ablation volume size and tumor ablation amount. This value difference divided by the average value for the respective ablation data serves as an indicator to see if the second property changes the primary property's influence on

the ablation area. After obtaining an overview about the parameter space, the individual tissue property configurations were investigated in the 2D and 3D spatial visualizations.

Ensemble C: The third ensemble dataset is characterized by changes in tumor size and, thus, aims at investigating the influence of the spatial distribution as well as the absolute size of the tumor. While the workflow is relatively similar to the analyses of the previously described datasets, a special focus lies on the spatial visualizations to understand the influence of the tumor's size and shape.

Ensemble D: For the creation of the fourth ensemble dataset, the position of the tumor and the vessels is varied. To achieve meaningful results, the needle position of the ablation instrument is adapted according to the tumor position such that the needle tip is always in the same location within the tumor. Similar to the previous ensemble dataset, this one targets the analysis of spatial tissue distributions. As especially the position of the blood vessels is suspected to have a strong impact, their analysis is one of the core analysis goals. Again, the spatial visualizations are especially used for identifying spatial variations in the ablation volume and their dependencies on the tissue properties.

5.2. Analysis of Tissue Properties

To understand the data at hand, we first observe different runs in the spatial visualization to obtain a first understanding of size and location of the ablation zones with respect to the different tissues. One example of the 3D visualization is shown in Figure 5. We can clearly see that the spatial domain is characterized by a tumor (pink) that is located relatively close to some vessels (red). By visualizing the ablation volume (green), we observe that large parts of the tumor are ablated for the selected tissue properties, but there are also smaller parts outside the ablation volume. When varying the different tissue properties, we can observe changes in the shape and size of the ablation volume, which we will investigate more systematically in the following. In the following, we focus on the analysis of single tissue properties and their influence on the simulation outcome which is described by Ensemble A. Further insights and a more detailed analysis of the other ensembles can be found in the supplementary material.

We start by analyzing the *density* of the different tissues. Here, we find the lowest ablation volume size to be $12\,843.3\,\text{mm}^3$ and the largest one $12\,923.1\,\text{mm}^3$ resulting in a difference of $79.8\,\text{mm}^3$ and $\Delta_{abl\_vol} = 0.620$. The ablated volume for the tumor is even lower with only $2.95\,\text{mm}^3$ and $\Delta_{t\_abl} = 0.066$. These small variations make the density an almost negligible property.

The *heat capacity*'s impact on the ablation area is even smaller than that of the density. Here, we find $\Delta_{abl\_vol} = 0.421$ and $\Delta_{t\_abl} = 0.04$. We can further see in the ablation data plot in Figure 6 that the heat capacity of liver and tumor have approximately equal influence on the ablation volume size while the heat capacity of the vessel does not impact this quantity. When analyzing the mean change in ablation volume per heat capacity unit for the individual tissues, we can confirm this observation.

When investigating the influence of the *thermal conductivity*, we find a significantly higher impact than for the
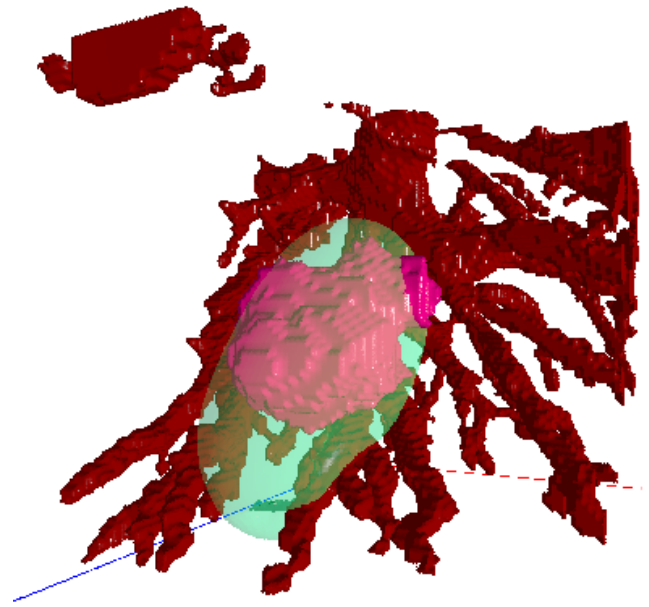

Figure 5: *3D spatial visualization: Blood vessels (red), tumor (pink), and ablation volume (green) are shown in a direct volume rendering for the simulation run with average tissue properties.*
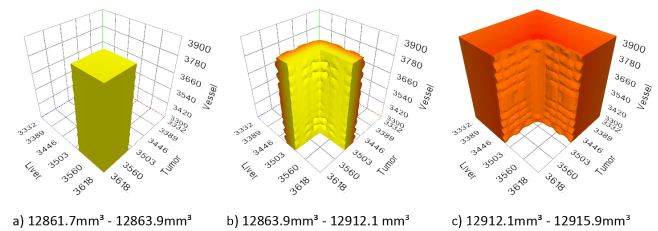

a) 12861.7mm³ - 12863.9mm³   b) 12863.9mm³ - 12912.1 mm³   c) 12912.1mm³ - 12915.9mm³

Figure 6: *Ablation data plot: The three surfaces display the coverage of the ablation volume size for heat capacity (color map as in Figure 1e). The vessels' heat capacity has no influence.*

previous properties ($\Delta_{abl\_vol} = 2.676$). While the highest impact is created by the thermal conductivity of the liver with $\Phi_{abl\_vol}^{tc} = -2.694\,\text{m}^3/(10^{-3}\text{W/mK})$, the tumor's and vessel's thermal conductivity also influence the ablation volume, but on a much smaller scale. Concerning the tumor ablation amount, the liver's and the tumor's thermal conductivity both affect it on a similar scale. However, while liver thermal conductivity decreases the ablation amount, the tumor's thermal conductivity increases it. The blood vessel's value has almost no effect on the tumor ablation.

The *relative blood perfusion rate* has by far the most influence on the size of the ablation area and the tumor ablation amount. The difference between the maximum and minimum ablation volume amounts to $13\,238\,\text{m}^3$, while the difference of the tumor ablation amount is $330.35\,\text{m}^3$. These high values result in $\Delta_{abl\_vol} = 103.661$ and $\Delta_{t\_abl} = 7.421$. For the analysis of this property only the liver and tumor tissue were inspected, since the blood perfusion of the blood vessels is
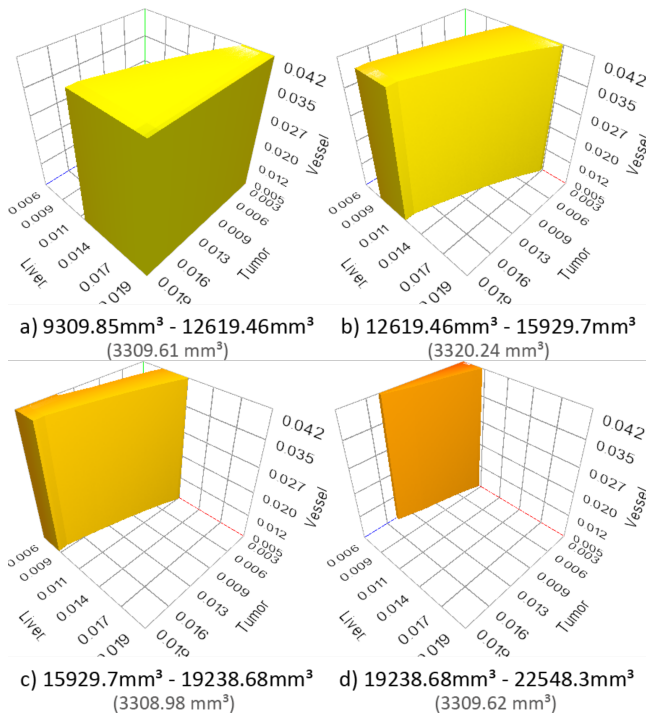
a) 9309.85mm³ - 12619.46mm³
(3309.61 mm³)

b) 12619.46mm³ - 15929.7mm³
(3320.24 mm³)

c) 15929.7mm³ - 19238.68mm³
(3308.98 mm³)

d) 19238.68mm³ - 22548.3mm³
(3309.62 mm³)

Figure 7: *Ablation data plot: Four surfaces of evenly sized ablation volume intervals for relative blood perfusion rate indicate that the higher the blood perfusion of the liver, the lower is its influence.*

a) 4199.95³ - 4282.53mm³
(85.58 mm³)

b) 4282.53mm³ - 4365.12mm³
(82.59 mm³)

c) 4365.12mm³ - 4447.71mm³
(82.59 mm³)

d) 4447.71mm³ - 4530.3mm³
(82.59 mm³)

Figure 8: *Ablation data plot: Four surfaces of evenly sized tumor ablation amount intervals for relative blood perfusion rate indicate the impact of the liver's and tumor's blood perfusion on the tumor ablation increases non-linearly with higher values.*

not supported by the simulation tool. It can be observed that the liver with $\Phi_{abl\_vol}^{bpr} = -77.329\,\mathrm{m}^3/(10^{-4}\mathrm{ml}/(\mathrm{s}\cdot\mathrm{cm}))$ has a way bigger impact on the ablation area than the tumor with a $\Phi_{abl\_vol}^{bpr} = -17.761\,\mathrm{m}^3/(10^{-4}\mathrm{ml}/(\mathrm{s}\cdot\mathrm{cm}))$. However, both tissue types have almost the same $\Phi_{t\_abl}^{bpr}$ value which suggests, that the smaller the liver's perfusion is, the higher the ablation of the healthy non-tumorous tissue.

Another important aspect is the high standard deviation for both Φ^{bpr} values. The surfaces in Figure 7 show that the higher the blood perfusion of the liver, the lower its influence on the ablation volume size. This can be concluded, because the ablation volume intervals of the four surfaces are all the same size, yet the coverage of the parameter space gets smaller. Therefore, one unit of the blood perfusion rate has more impact on the ablation volume when the surface is relatively small.

For the tumor ablation amount, the opposite is the case: the impact of the liver's and tumor's blood perfusion on the tumor ablation increases with higher values (see Figure 8). However, in both cases, we can observe a nonlinear change when changing the parameter range linearly. This can be identified by the varying sizes of the regions, while the parameter range stays the same size.

The inspection of the ablation volume in the spatial views of TPAT visualizes the effect of different blood perfusion rate values on the ablation area. In Figure 9, the effects of low and high blood perfusion values for the liver and tumor tissues can be seen. While the tumor's blood perfusion mostly affects the area around
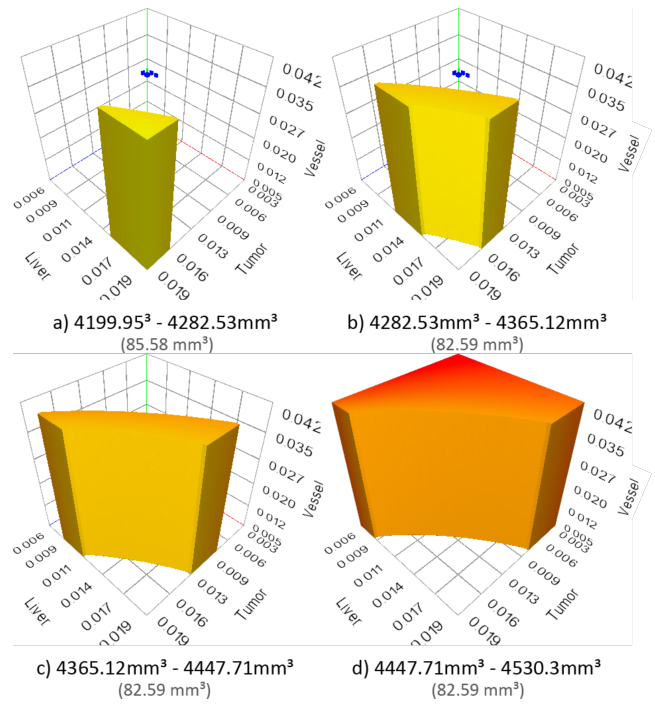
the tumor, the liver's blood perfusion leads to a more even expansion/reduction of the whole volume. However, in both cases, the change in proximity to the blood vessel is minimal in the selected slice, which indicates the strong effect blood vessels have on the ablation process.

Closer inspection of the volume discloses that the impact of the blood perfusion rate greatly decreases in the proximity of blood vessels. Also, when the ablation volume is up close to a blood vessel, like in Figure 10, the blood perfusion rate of the liver has close to no influence on that portion of the ablation volume. Neither low nor high blood perfusion values seem to affect these parts.

5.3. Domain Expert Feedback

We developed our tool in close collaboration with domain experts (one professor, one post-doc, and one student) who developed the simulation tool. In several joint sessions, we discussed our approach and iteratively integrated their feedback. The close collaboration in the design process helped us to address the needs of the domain scientist, for example, by incorporating domain-specific measures. In the end, we provided our tool to them for experimenting by themselves and collected feedback.

The tool allowed them to confirm their hypotheses about the different influences of the various tissue properties as well as the influences of the tissues. They also appreciated the spatial visualizations because they clearly showed the impact of the position of the ves-
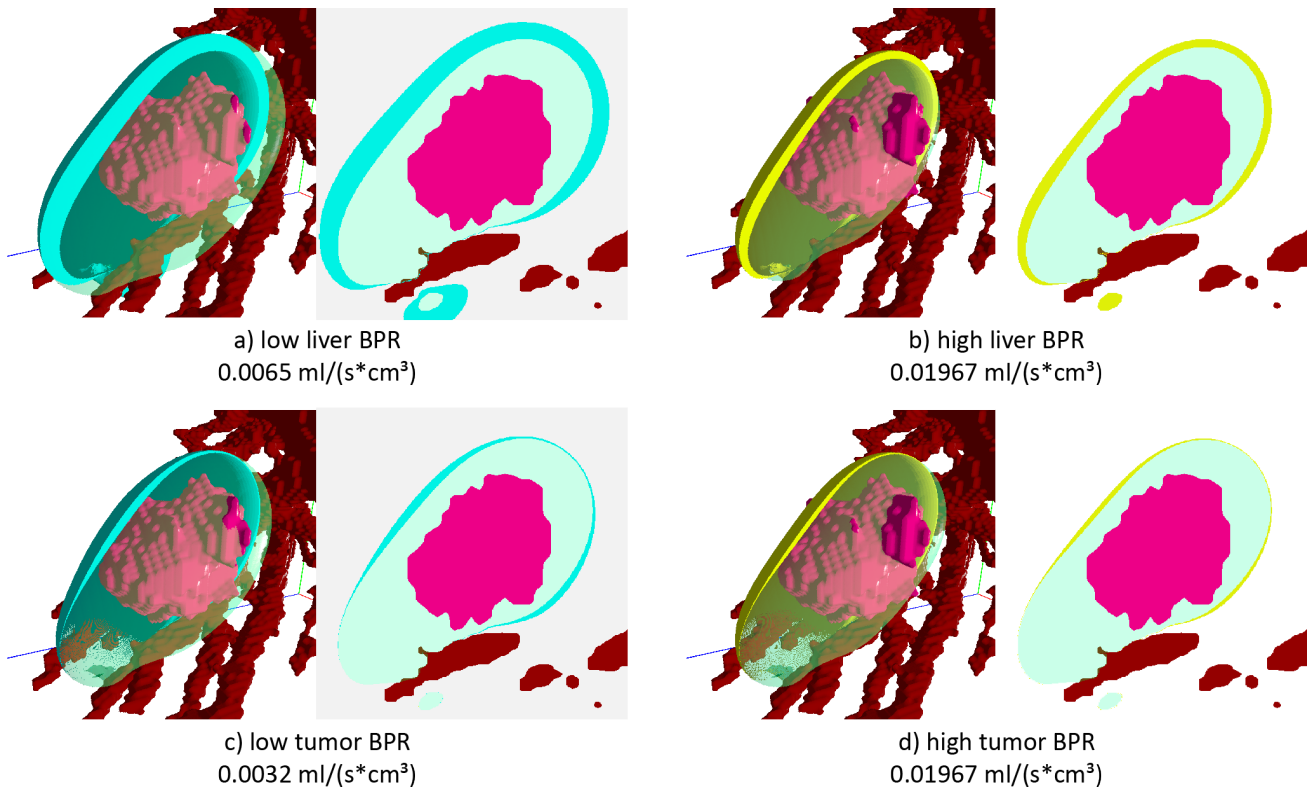
a) low liver BPR
0.0065 ml/(s*cm³)

b) high liver BPR
0.01967 ml/(s*cm³)

c) low tumor BPR
0.0032 ml/(s*cm³)

d) high tumor BPR
0.01967 ml/(s*cm³)

Figure 9: *2D and 3D spatial visualizations for comparing ablation volume when changing blood perfusion rate. 3D volumes have been clipped to better observe the thickness of the ablation volume expansion (cyan) and reduction (yellow). While the tumor's blood perfusion mostly affects the area around the tumor (bottom), the liver's blood perfusion leads to a more even expansion/reduction of the whole volume (top). However, the cooling effect of vessels can be observed in both cases.*

sels. In contrast to pure numerical values, our approach allows them to visually investigate the spatial variations. They were also interested in the nonlinearity of the dependencies. The ablation data plot showed them that a linear change in the tissue properties might lead to nonlinear variations in the ablation quantities like the size of the ablated volume.

However, they noted that handling large amounts of data is challenging and suggested to allow running simulations directly from the tool based on the previous analysis. We plan to investigate these features in the future.

6. Discussion

The use case has shown that the program allows the user to easily explore large datasets of RF ablation data while also providing an in-depth analysis of individual ablation volumes. As stated in the beginning, we can assume that our simulations use three tissues: vessels, healthy tissue (in our case the liver), and malignant tissue (in our case a tumor). However, for a broader generalizability beyond RF ablation, an extension to more than three tissues would be helpful. While one could tackle this challenge by interactively switching the axes in our ablation data plot, this would still only visualize a three-dimensional parameter subspace. Therefore, the

generalization to higher dimensions, which was beyond the scope of this paper, remains an open challenge.

In general, our tool scales well with the number of ensemble members. We considered ensembles with 96 to 225 ensemble members. As the different ablation metrics are precomputed, the number of ensemble members does not influence the spatial visualizations directly. The ablation data plot also scales well with the number of tissue properties. However, as the spatial visualizations make use of interpolation, a high number of ensemble members when combined with a high resolution might lead to delays. For the ensembles investigated in this work, we did not experience any problems. As extremely large simulation ensembles are costly to compute, our tool works well for common ensemble sizes.

7. Conclusion

In this work, we presented a tissue property analysis tool *TPAT* that supports the interactive visual analysis of tissue properties in radiofrequency ablation simulations. We create spatial visualizations to compare different tissue properties and investigate their influence together with parameter space visualizations that allow us to analyze a whole ensemble. In our discussion with domain experts, the tool was found suitable for the described kind of analyses. The tool allows for a better analysis of the influence of tissue properties,
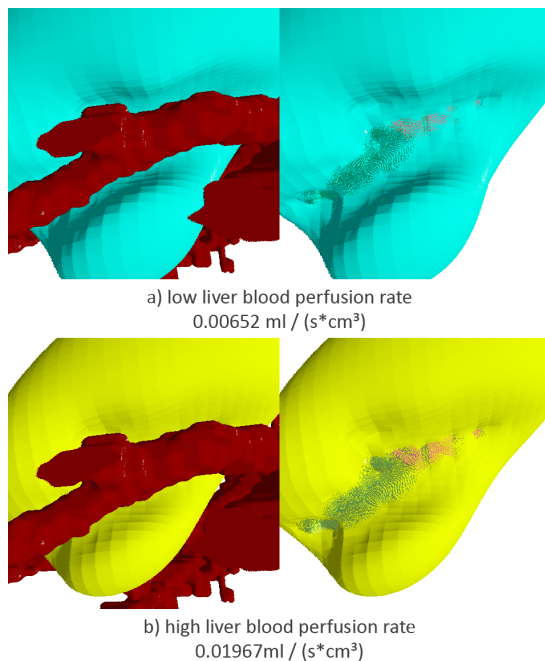
a) low liver blood perfusion rate
0.00652 ml / (s*cm³)

b) high liver blood perfusion rate
0.01967ml / (s*cm³)

Figure 10: *Zoomed-in comparative volume visualizations of runs with low and high liver blood perfusion rates exhibit that there is no influence close to blood vessels.*

which supports the identification of the most important properties as well as the spatial regions where the influence is largest. Therefore, one can identify the important aspects that should be included in clinical treatments. Although our approach targets RF ablation, it can be easily applied to other treatment methods to detect and analyze relevant parameters in respective simulations, as most of our visualizations are generally applicable.

For future work, our approach can be further improved by allowing a progressive ensemble analysis and executing simulations directly from the visualization tool. Based on the experts feedback, this might lead to significant improvements in their analysis workflow. The visualization of ablation metrics for more than three tissue types as well as including uncertainty in the segmentation is also left for future work. The approach would further benefit from a structured user evaluation with additional researchers that were not directly involved in the development of the tool.

Acknowledgments

References

[ALHG08] AHMED M., LIU Z., HUMPHRIES S., GOLDBERG S. N.: Computer modeling of the combined effects of perfusion, electrical conductivity, and thermal conductivity on tissue heating patterns in radiofrequency tumor ablation. *International Journal of Hyperthermia 24*, 7 (2008), 577–588. doi:10.1080/02656730802192661.

[Ber06] BERJANO E.: Theoretical modeling for radiofrequency ablation: State-of-the-art and challenges for the future. *Biomedical engineering online 5* (02 2006), 24. doi:10.1186/1475-925X-5-24.

[BKM*06] BRICAULT I., KIKINIS R., MORRISON P. R., VANSONNENBERG E., TUNCALI K., SILVERMAN S. G.: Liver metastases: 3D shape-based analysis of CT scans for detection of local recurrence after radiofrequency ablation. *Radiology 241*, 1 (Oct. 2006), 243–250. doi:10.1148/radiol.2411050987.

[BM10] BRUCKNER S., MÖLLER T.: Result-driven exploration of simulation parameter spaces for visual effects design. *IEEE Transactions on Visualization and Computer Graphics 16*, 6 (2010), 1468–1476. doi:10.1109/tvcg.2010.190.

[BPM*15] BOCK A., PEMBROKE A., MAYS M. L., RASTAETTER L., ROPINSKI T., YNNERMAN A.: Visual verification of space weather ensemble simulations. In *2015 IEEE Scientific Visualization Conference (SciVis)* (2015), IEEE, pp. 17–24. doi:10.1109/SciVis.2015.7429487.

[Buh00] BUHMANN M. D.: Radial basis functions. *Acta Numerica 9* (2000), 1–38. doi:10.1017/S0962492900000015.

[Dic45] DICE L. R.: Measures of the amount of ecologic association between species. *Ecology 26*, 3 (1945), 297–302. URL: http://www.jstor.org/stable/1932409.

[EL22] EVERS M., LINSEN L.: Multi-dimensional parameter-space partitioning of spatio-temporal simulation ensembles. *Computers & Graphics 104* (2022), 140–151. doi:10.1016/j.cag.2022.04.005.

[FKRW17] FERSTL F., KANZLER M., RAUTENHAUS M., WESTERMANN R.: Time-hierarchical clustering and visualization of weather forecast ensembles. *IEEE Transactions on Visualization and Computer Graphics 23*, 1 (2017), 831–840. doi:10.1109/tvcg.2016.2598868.

[HHB16] HAO L., HEALEY C. G., BASS S. A.: Effective visualization of temporal ensembles. *IEEE Transactions on Visualization and Computer Graphics 22*, 1 (2016), 787–796. doi:10.1109/tvcg.2015.2468093.

[KAP*06] KRÖGER T., ALTROGGE I., PREUSSER T., PEREIRA P. L., SCHMIDT D., WEIHUSEN A., PEITGEN H.-O.: Numerical simulation of radio frequency ablation with state dependent material parameters in three space dimensions. In *International Conference on Medical Image Computing and Computer-Assisted Intervention – MICCAI 2006* (2006), Larsen R., Nielsen M., Sporring J., (Eds.), Lecture Notes in Computer Science, Springer, pp. 380–388. doi:10.1007/11866763_47.

[KBL19a] KAPPE C., BÖTTINGER M., LEITTE H.: Analysis of decadal climate predictions with user-guided hierarchical ensemble clustering. *Computer Graphics Forum 38*, 3 (2019), 505–515. doi:10.1111/cgf.13706.

[KBL19b] KAPPE C. P., BOTTINGER M., LEITTE H.: Exploring variability within ensembles of decadal climate predictions. *IEEE Transactions on Visualization and Computer Graphics 25*, 3 (2019), 1499–1512. doi:10.1109/tvcg.2018.2810919.

[ME19] MA B., ENTEZARI A.: An interactive framework for visualization of weather forecast ensembles. *IEEE Transactions on Visualization and Computer Graphics 25*, 1 (2019), 1091–1101. doi:10.1109/tvcg.2018.2864815.

[OBJ15] OBERMAIER H., BENSEMA K., JOY K. I.: Visual trends analysis in time-varying ensembles. *IEEE Transactions on Visualization and Computer Graphics 22*, 10 (2015), 2331–2342. doi:10.1109/tvcg.2015.2507592.

[OKB*19] ORBAN D., KEEFE D. F., BISWAS A., AHRENS J., ROGERS D.: Drag and track: A direct manipulation interface for contextualizing data instances within a continuous parameter space. *IEEE Transactions on Visualization and Computer Graphics 25*, 1 (2019), 256–266. doi:10.1109/tvcg.2018.2865051.

[PBCR11] PRETORIUS A. J., BRAY M.-A., CARPENTER A. E., RUDDLE R. A.: Visualization of parameter space for image analysis. *IEEE*

Transactions on Visualization and Computer Graphics 17, 12 (2011), 2402–2411. doi:10.1109/tvcg.2011.253.

[PPA*12] PHADKE M. N., PINTO L., ALABI O., HARTER J., TAY-LOR II R. M., WU X., PETERSEN H., BASS S. A., HEALEY C. G.: Exploring ensemble visualization. In *Visualization and Data Analysis 2012* (2012), vol. 8294, International Society for Optics and Photonics, p. 82940B. doi:10.1117/12.912419.

[PWB*09] POTTER K., WILSON A., BREMER P.-T., WILLIAMS D., DOUTRIAUX C., PASCUCCI V., JOHNSON C. R.: Ensemble-vis: A framework for the statistical visualization of ensemble data. In *2009 IEEE International Conference on Data Mining Workshops* (2009), IEEE, pp. 233–240. doi:10.1109/ICDMW.2009.55.

[RCMM*16] RAIDOU R., CASARES-MAGAZ O., MUREN L., VAN DER HEIDE U., RØRVIK J., BREEUWER M., VILANOVA A.: Visual analysis of tumor control models for prediction of radiotherapy response. *Computer Graphics Forum 35*, 3 (June 2016), 231–240. URL: https://doi.org/10.1111/cgf.12899, doi:10.1111/cgf.12899.

[RGH*19] RISTOVSKI G., GARBERS N., HAHN H., PREUSSER T., LINSEN L.: Uncertainty-aware visual analysis of radiofrequency ablation simulations. *Computers & Graphics 79* (April 2019), 24–35. doi:10.1016/j.cag.2018.12.005.

[RWS*10] RIEDER C., WEIHUSEN A., SCHUMANN C., ZIDOWITZ S., PEITGEN H.-O.: Visual support for interactive post-interventional assessment of radiofrequency ablation therapy. *Computer Graphics Forum 29*, 3 (Aug. 2010), 1093–1102. doi:10.1111/j.1467-8659.2009.01665.x.

[SCTL05] SHEU T. W. H., CHOU C. W., TSAI S. F., LIANG P. C.: Three-dimensional analysis for radio-frequency ablation of liver tumor with blood perfusion effect. *Computer Methods in Biomechanics and Biomedical Engineering 8*, 4 (Aug 2005), 229–40. doi:10.1080/10255840500289731.

[SHB*14] SEDLMAIR M., HEINZL C., BRUCKNER S., PIRINGER H., MÖLLER T.: Visual parameter space analysis: A conceptual framework. *IEEE Transactions on Visualization and Computer Graphics 20*, 12 (2014), 2161–2170. doi:10.1109/tvcg.2014.2346321.

[She68] SHEPARD D.: A two-dimensional interpolation function for irregularly-spaced data. In *Proceedings of the 1968 23rd ACM National Conference* (New York, NY, USA, 1968), ACM '68, ACM, pp. 517–524. doi:10.1145/800186.810616.

[STDS95] SPENCE B., TWEEDIE L., DAWKES H., SU H.: Visualization for functional design. In *Proceedings of the 1995 IEEE Symposium on Information Visualization* (Washington, DC, USA, 1995), INFOVIS '95, IEEE Computer Society, pp. 4–10. doi:10.1109/infvis.1995.528680.

[SZD*10] SANYAL J., ZHANG S., DYER J., MERCER A., AMBURN P., MOORHEAD R.: Noodles: A tool for visualization of numerical weather model ensemble uncertainty. *IEEE Transactions on Visualization and Computer Graphics 16*, 6 (2010), 1421–1430. doi:10.1109/TVCG.2010.181.

[WHLS19] WANG J., HAZARIKA S., LI C., SHEN H.-W.: Visualization and visual analysis of ensemble data: A survey. *IEEE Transactions on Visualization and Computer Graphics 25*, 9 (2019), 2853–2872. doi:10.1109/tvcg.2018.2853721.

[WLSL17] WANG J., LIU X., SHEN H.-W., LIN G.: Multi-resolution climate ensemble parameter analysis with nested parallel coordinates plots. *IEEE Transactions on Visualization and Computer Graphics 23*, 1 (2017), 81–90. doi:10.1109/tvcg.2016.2598830.